Theory of Hall effect in two-dimensional giant Rashba systems

Hidekatsu Suzuura[1,*] and Tsuneya Ando[2]

[1]*Division of Applied Physics, Graduate School of Engineering, Hokkaido University, Sapporo 060-8628, Japan*

[2]*Department of Physics, Tokyo Institute of Technology, 2-12-1 Ookayama, Tokyo 152-8551, Japan*

(Received 15 January 2016; published 12 July 2016)

The weak-field Hall conductivity of disordered two-dimensional systems with strong Rashba spin-orbit interaction is studied in a self-consistent Born approximation. Explicit numerical results are obtained for scatterers with a Gaussian potential and for charged impurities. The singular behavior associated with a conelike crossing band appears only in the case of scatterers with a long-range Gaussian potential, which do not cause mixing with the outer band. In the case of more realistic scatterers such as charged impurities, the singularity is completely removed except the presence of a weak steplike feature. The Hall conductivity associated with the spin-Zeeman energy is also strongly reduced by interband mixing and generally remains much smaller than the orbital contribution.

DOI: 10.1103/PhysRevB.94.035302

I. INTRODUCTION

Systems with a giant spin splitting due to a Rashba-type spin-orbit interaction attract much attention [1], from the viewpoint of spintronics applications as well as fundamental physics [2]. In a topological insulator Bi_2S_3, for example, spin splitting much larger than in III-V and II-VI semiconductors was realized and its electrostatic control was demonstrated [3]. More recently, much larger splitting was realized in the bulk of polar semiconductor BiTeI [4–10], and a two-dimensional electronic system on its surface is shown to exist [11,12]. In this paper, we theoretically study the weak-field Hall effect of two-dimensional systems with the Rashba spin-orbit interaction in the presence of nonzero-range impurities based on a self-consistent Born approximation.

In a Rashba system, there appears a conelike crossing point at $\boldsymbol{k} = 0$, where spin splitting vanishes [13–15]. In this vicinity, the electron motion is governed by Weyl's equation for a neutrino or the Dirac equation in the relativistic limit, as in monolayer graphene [16–21]. Transport quantities in the Weyl system of graphene are known to exhibit singular and intriguing behaviors in the vicinity of the band crossing point as have been discussed in various reviews [22–26]. Typical examples are a universal minimum conductivity, predicted theoretically [27] and discussed experimentally [28], diamagnetic susceptibility given by a δ function [16,29–32], and the absence of backscattering [33–35].

Effects of disorder on transport in Weyl systems have been studied for scatterers with potential range smaller than typical electron wavelength in a self-consistent Born approximation [27,36–38], and within approximations assuming energy-independent broadening [39–45]. Recently, the scheme based on the self-consistent Born approximation was extended to the case of scatterers with long-range potential [46–54]. In this paper, we use this new scheme to calculate the Hall conductivity in a giant Rashba system.

The paper is organized as follows: In Sec. II, following a brief review on the electronic states, we discuss the method to calculate the Hall conductivity for long-range scatterers in the Boltzmann transport theory and in the self-consistent Born approximation. In Sec. III some examples of numerical results are presented for scatterers with a Gaussian potential and for charged impurities. A brief discussion is given in Sec. IV and a short summary is given in Sec. V.

II. FORMULATION

A. Effective-mass description

We consider a two-dimensional system, described by the Hamiltonian

$$\mathcal{H}_0 = \frac{\hbar^2\hat{\boldsymbol{k}}^2}{2m} + \frac{\hbar^2 k_{\rm so}}{m}(\hat{\boldsymbol{k}} \times \boldsymbol{\sigma}) \cdot \boldsymbol{n}, \tag{1}$$

with $\hat{\boldsymbol{k}} = -i\nabla$, $\boldsymbol{n}$ being a unit vector perpendicular to the system, and Pauli spin matrices $\boldsymbol{\sigma} = (\sigma_x, \sigma_y)$ and σ_z, where m is the effective mass and $k_{\rm so}$ represents the wave number characterizing the strength of the spin-orbit interaction. As the corresponding typical energy, we introduce

$$\varepsilon_{\rm so} \equiv \frac{\hbar^2 k_{\rm so}^2}{2m}. \tag{2}$$

For a given energy ε above the band minimum $-\varepsilon_{\rm so}$, we have

$$k_\pm = \sqrt{\frac{2m}{\hbar^2}[\varepsilon + 2\varepsilon_{\rm so} \pm 2\sqrt{\varepsilon_{\rm so}(\varepsilon + \varepsilon_{\rm so})}]}, \tag{3}$$

where k_+ and k_- denote the wave vector of the outer and inner band, respectively. The corresponding density of states becomes

$$D_\pm(\varepsilon) = \frac{1}{2\pi}\left|\frac{k_\pm \partial k_\pm}{\partial \varepsilon}\right| = \frac{m}{2\pi\hbar^2}\left|1 \pm \sqrt{\frac{\varepsilon_{\rm so}}{\varepsilon + \varepsilon_{\rm so}}}\right|\theta(\varepsilon + \varepsilon_{\rm so}), \tag{4}$$

where we have defined a step function

$$\theta(t) = \begin{cases} 1 & (t \geqslant 0); \\ 0 & (t < 0). \end{cases} \tag{5}$$

*suzuura@eng.hokudai.ac.jp

The total density of states becomes

$$D(\varepsilon) = \sum_{\pm} D_{\pm}(\varepsilon) = \begin{cases} \dfrac{m}{\pi\hbar^2} & (\varepsilon > 0); \\ \dfrac{m}{\pi\hbar^2}\sqrt{\dfrac{\varepsilon_{\rm so}}{\varepsilon+\varepsilon_{\rm so}}} & (-\varepsilon_{\rm so} < \varepsilon < 0). \end{cases} \tag{6}$$

In the region $\varepsilon > 0$, it is exactly the same as that in a two-dimensional system free from spin-orbit interaction, i.e., $k_{\rm so} = 0$, becomes larger in the region $\varepsilon < 0$, and diverges at the band bottom $\varepsilon = -\varepsilon_{\rm so}$. It has a kinklike structure at $\varepsilon = 0$ corresponding to the linearly vanishing density of states of the conelike inner band. The electron concentration or the carrier density is given by

$$n_{\rm s}(\varepsilon) = \begin{cases} n_{\rm so}\left(\frac{\varepsilon}{\varepsilon_{\rm so}} + 2\right) & (\varepsilon > 0); \\ 2n_{\rm so}\sqrt{1 + \frac{\varepsilon}{\varepsilon_{\rm so}}} & (-\varepsilon < \varepsilon < 0), \end{cases} \tag{7}$$

with

$$n_{\rm so} = \frac{m}{\pi\hbar^2\varepsilon_{\rm so}} = \frac{k_{\rm so}^2}{2\pi}, \tag{8}$$

corresponding to the electron concentration at $\varepsilon = \varepsilon_{\rm so}$ in the system free from spin-orbit interaction.

The group velocity becomes

$$\boldsymbol{v}_{\boldsymbol{k}_\pm} = v_\pm(\varepsilon)\frac{\boldsymbol{k}_\pm}{k_\pm}, \tag{9}$$

with

$$v_\pm(\varepsilon) = \frac{1}{\hbar}\left(\frac{\partial k_\pm}{\partial\varepsilon}\right)^{-1} = \frac{\hbar k_\pm}{m}\left(1 \pm \sqrt{\frac{\varepsilon_{\rm so}}{\varepsilon+\varepsilon_{\rm so}}}\right)^{-1}. \tag{10}$$

The cyclotron frequency becomes

$$\omega_\pm = \frac{1}{l^2}\frac{v_\pm}{k_\pm} = \omega_{\rm c}\left(1 \pm \sqrt{\frac{\varepsilon_{\rm so}}{\varepsilon+\varepsilon_{\rm so}}}\right)^{-1}, \tag{11}$$

where l is the magnetic length and $\omega_{\rm c}$ is the cyclotron frequency, defined by

$$l^2 = \frac{c\hbar}{eB}, \quad \omega_{\rm c} = \frac{eB}{mc}, \tag{12}$$

with $B = |\boldsymbol{B}|$, where $\boldsymbol{B}$ is the magnetic field perpendicular to the system. For the band corresponding to k_-, the velocity changes its sign at zero energy and the cyclotron frequency is singular like $\propto \varepsilon^{-1}$, i.e., it diverges at $\varepsilon = 0$ and changes its sign. Some of the quantities characterizing the electron motion are shown in Fig. 1.

In the presence of scatterers, the Hamiltonian becomes

$$\mathcal{H} = \mathcal{H}_0 + V(\boldsymbol{r}), \tag{13}$$

with

$$V(\boldsymbol{r}) = \sum_j u_{\rm i}(\boldsymbol{r}-\boldsymbol{r}_j)\begin{pmatrix} 1 & 0 \\ 0 & 1, \end{pmatrix} \tag{14}$$

where $u_{\rm i}(\boldsymbol{r})$ is the impurity potential assumed to be independent of the electron spin and $\boldsymbol{r}_j$ is the position of the jth impurity. In the following, we shall confine ourselves to the case of isotropic potential, i.e.,

$$u_{\rm i}(\boldsymbol{r}) = \int \frac{d\boldsymbol{q}}{(2\pi)^2} u_{\rm i}(q) e^{i\boldsymbol{q}\cdot\boldsymbol{r}}, \tag{15}$$

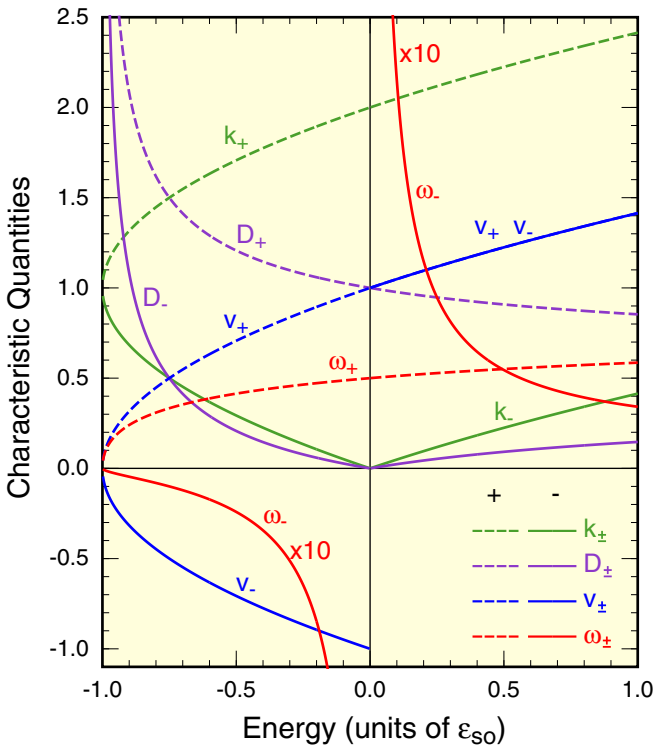

FIG. 1. Wave vectors $k_\pm/k_{\rm so}$, partial densities of states $D_\pm(\varepsilon)(m/\pi\hbar^2)^{-1}$, group velocities $v_\pm(\hbar k_{\rm so}/m)^{-1}$, and cyclotron frequencies $\omega_\pm/\omega_{\rm c}$ as a function of energy.

with real $u_{\rm i}(\boldsymbol{q}) = u_{\rm i}(q)$ ($q = |\boldsymbol{q}|$). Extension to anisotropic impurities is straightforward as long as isotropy is recovered after averaging over impurity configurations.

B. Boltzmann equation

To the lowest order in applied electric field $\boldsymbol{E}$, the Boltzmann equation for the distribution function $g(\boldsymbol{k}_s)$ with $s = \pm$ is given by

$$\begin{aligned}(-e)\boldsymbol{E}\cdot\boldsymbol{v}_{\boldsymbol{k}_s}\left(-\frac{\partial f}{\partial\varepsilon_{\boldsymbol{k}_s}}\right) = \sum_{s'}\int\frac{d\boldsymbol{k}_{s'}}{(2\pi)^2}\frac{2\pi}{\hbar}n_{\rm i}|\langle\boldsymbol{k}_{s'}|u_{\rm i}|\boldsymbol{k}_s\rangle|^2 \\ \times\delta[\varepsilon(k_s)-\varepsilon(k_{s'})][g(\boldsymbol{k}_s)-g(\boldsymbol{k}_{s'})] \\ -\frac{e}{c\hbar}\left(\boldsymbol{v}_{\boldsymbol{k}_s}\times\boldsymbol{B}\right)\cdot\frac{\partial g(\boldsymbol{k}_s)}{\partial\boldsymbol{k}_s},\end{aligned} \tag{16}$$

where $f(\varepsilon)$ is the Fermi distribution function and $n_{\rm i}$ is the concentration of scatterers. This can be solved in the way similar to that in the case of bilayer graphene [51,53], for example, giving the diagonal conductivity $\sigma \equiv \sigma_{xx}$ in the absence of a magnetic field and the off-diagonal Hall conductivity σ_{xy} to the linear order in magnetic-field strength B. In the following, we shall write the conductivity components as

$$\sigma_{\mu\nu} = \int d\varepsilon\left(-\frac{\partial f}{\partial\varepsilon}\right)\sigma_{\mu\nu}(\varepsilon), \tag{17}$$

with $\mu = x, y$ and $\nu = x, y$.

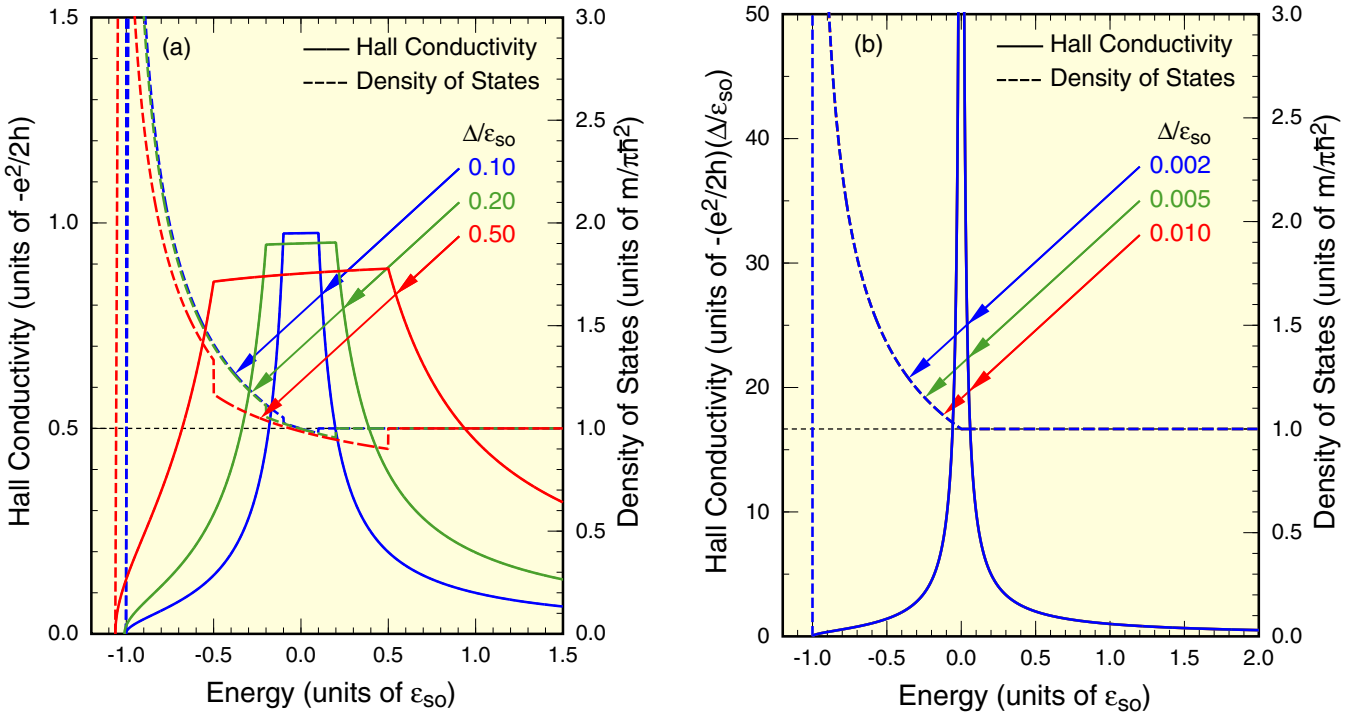

FIG. 2. Calculated density of states and spin-Zeeman Hall conductivity in an ideal system. (a) The case of relatively large gap. (b) Close to the small-gap limit.

C. Spin-Zeeman Hall conductivity

In addition to the orbital contribution, in general, we have to include the spin-Zeeman energy

$$\mathcal{H} \to \mathcal{H} + \Delta\sigma_z, \tag{18}$$

$$\Delta = \frac{g}{2}\mu_B B, \tag{19}$$

into the Hamiltonian, where g is the effective g factor and $\mu_B = e\hbar/(2m_0c)$, where m_0 is the free-electron mass. This gives rise to the opening of gap $2|\Delta|$ at $k = 0$ and the resulting off-diagonal conductivity is often called the anomalous Hall conductivity [55–82].

The Hall conductivity is written as

$$\sigma_{xy} = -i\frac{\hbar e^2}{L^2}\sum_{\alpha} f(\varepsilon_\alpha)\sum_{\beta\neq\alpha}\frac{(v_x)_{\alpha\beta}(v_y)_{\beta\alpha} - (v_y)_{\alpha\beta}(v_x)_{\beta\alpha}}{(\varepsilon_\alpha - \varepsilon_\beta)^2}, \tag{20}$$

where L^2 is the system area, α and β denote eigenstates with eigenenergies ε_α and ε_β, respectively, and v_x and v_y are the velocity in the x and y directions, respectively. In the ideal system, we can easily calculate the above and have

$$\sigma_{xy}(\varepsilon) = \begin{cases} -\frac{e^2}{2h}[g_-(\varepsilon) - g_+(\varepsilon)] & (\varepsilon_{\min} < \varepsilon < -|\Delta|); \\ -\frac{e^2}{2h}\left[\frac{\Delta}{|\Delta|} - g_+(\varepsilon)\right] & (-|\Delta| < \varepsilon < +|\Delta|); \\ -\frac{e^2}{2h}[-g_-(\varepsilon) - g_+(\varepsilon)] & (\varepsilon > +|\Delta|), \end{cases} \tag{21}$$

where

$$g_\pm(\varepsilon) \equiv \frac{1}{2}\frac{\Delta}{\varepsilon_{\rm so} \pm \sqrt{\varepsilon_{\rm so}(\varepsilon - \varepsilon_{\min})}}, \tag{22}$$

$$\varepsilon_{\min} = -\varepsilon_{\rm so} - \frac{\Delta^2}{4\varepsilon_{\rm so}}. \tag{23}$$

In the limit of $\Delta \to 0$, we have

$$\sigma_{xy}(\varepsilon) = -\frac{e^2}{2h}\Delta\left[2\delta(\varepsilon) + \frac{1}{\varepsilon}\theta(\varepsilon) - \frac{1}{\varepsilon}\sqrt{1 + \frac{\varepsilon}{\varepsilon_{\rm so}}}\theta(-\varepsilon)\theta(\varepsilon + \varepsilon_{\rm so})\right]. \tag{24}$$

In the vicinity of zero energy, this diverges like $\sigma_{xy} \sim -(e^2/2h)(\Delta/|\varepsilon|)$ and the δ-function term is less important. This expression gives the spin-Zeeman Hall conductivity proportional to B by the replacement $\Delta \to (g/2)\mu_B B$.

Figure 2 shows the spin-Zeeman Hall conductivity in ideal systems without any scatterers with various gaps at $k = 0$. As shown in Fig. 2(a), within the opened gap, the Hall conductivity is close to $-e^2/2h$ and its absolute value decreases with the increase of the gap. In the limit of vanishing gap shown in Fig. 2(b), the Hall conductivity becomes proportional to $\Delta/|\varepsilon|$ near $\varepsilon = 0$.

This spin-Zeeman Hall conductivity corresponds with the intrinsic contribution for the anomalous Hall conductivity in a system without disorder where the energy gap $2|\Delta|$ is induced by a spontaneous magnetization in the absence of the magnetic field [62,70]. In the following sections, we discuss the weak-field Hall conductivity proportional to the magnetic field B,

while the analytical expression of Eq. (21) is valid for Δ of arbitrary strength.

D. Conductivity formula

According to the Kubo formula [83], the diagonal conductivity is written as

$$\sigma_{xx}(\varepsilon) = \frac{e^2}{2\pi\hbar L^2}\mathrm{Re\,Tr}[\mathcal{H}_x\mathcal{G}(+)\mathcal{H}_x\mathcal{G}(-) - \mathcal{H}_x\mathcal{G}(+)\mathcal{H}_x\mathcal{G}(+)], \tag{25}$$

where we have introduced Green's operator

$$\mathcal{G}(\pm) \equiv \mathcal{G}(\varepsilon \pm i0) = \frac{1}{\varepsilon - \mathcal{H} \pm i0}, \tag{26}$$

and have defined

$$\mathcal{H}_x = \frac{\partial\mathcal{H}}{\partial k_x}, \quad \mathcal{H}_y = \frac{\partial\mathcal{H}}{\partial k_y}. \tag{27}$$

A theoretical scheme to calculate the weak-field Hall conductivity due to orbital cyclotron motion proportional to applied magnetic field, based on the Kubo formula, was developed by Fukuyama and coworkers [84,85]. The Hall conductivity is separated into two terms:

$$\sigma_{xy}(\varepsilon) = \sigma'_{xy}(\varepsilon) + \sigma''_{xy}(\varepsilon), \tag{28}$$

with

$$\sigma'_{xy}(\varepsilon) = \frac{e^2\hbar^3}{\pi l^2}H_{xy}(\varepsilon), \tag{29}$$

$$\sigma''_{xy}(\varepsilon) = \frac{2e^2\hbar^3}{\pi l^2}\int_{-\infty}^{\varepsilon} H'_{xy}(\varepsilon')\,d\varepsilon', \tag{30}$$

which are linear in magnetic field strength B. Here, we have

$$H_{xy} = -\frac{1}{\hbar^4 L^2}\mathrm{Tr\,Im}\,\mathcal{H}_x\mathcal{G}(+)\mathcal{H}_y\mathcal{G}(+)\mathcal{H}_x\mathcal{G}(+)\mathcal{H}_y\mathcal{G}(-), \tag{31}$$

$$H'_{xy} = -\frac{1}{\hbar^4 L^2}\mathrm{Tr\,Im}\,\mathcal{H}_x\mathcal{G}(+)^2\mathcal{H}_y\mathcal{G}(+)\mathcal{H}_x\mathcal{G}(+)\mathcal{H}_y\mathcal{G}(+), \tag{32}$$

with

$$\mathcal{H}_{xx} = \mathcal{H}_{yy} = \frac{\partial^2\mathcal{H}}{\partial k_x^2} = \frac{\hbar^2}{m}. \tag{33}$$

The Hall coefficient is defined by

$$R_{\mathrm{H}} = \frac{\sigma_{xy}}{B\sigma_{xx}^2}. \tag{34}$$

In the absence of the spin-orbit interaction, $R_{\mathrm{H}} = -1/(n_{\mathrm{s}}ec)$ within the Boltzmann theory, where n_{s} is the carrier concentration.

For the Hall conductivity due to the spin-Zeeman energy, it is sufficient to calculate the conductivity in the presence of nonzero gap Δ and consider the case of sufficiently small Δ. The Hall conductivity is given by Eq. (28) with

$$\sigma'_{xy}(\varepsilon) = \frac{e^2}{2\pi\hbar L^2}\mathrm{Tr\,Re}\,\mathcal{H}_x\mathcal{G}(+)\mathcal{H}_y\mathcal{G}(-), \tag{35}$$

$$\sigma''_{xy}(\varepsilon) = \frac{e^2}{\pi\hbar L^2}\int_{-\infty}^{\varepsilon} d\varepsilon'\,\mathrm{Tr\,Re}\,\mathcal{H}_x\mathcal{G}(+)^2\mathcal{H}_y\mathcal{G}(+). \tag{36}$$

These formulas give identically vanishing results for $\Delta = 0$.

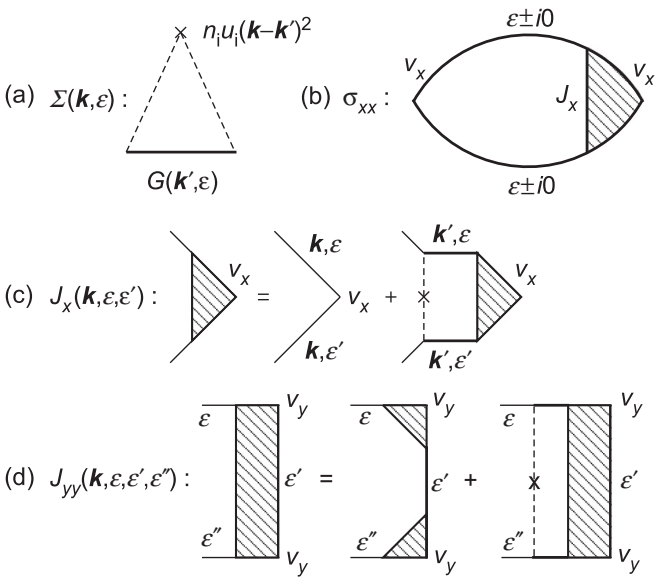

FIG. 3. The Feynman diagrams for (a) the self-energy, (b) the diagonal conductivity, (c) the current-vertex function, and (d) the double-vertex function in the self-consistent Born approximation.

E. Self-consistent Born approximation

The Green's function averaged over impurity configuration becomes a (2,2) matrix and is given by

$$G(\boldsymbol{k},\varepsilon) = \frac{1}{\varepsilon - \mathcal{H}_0(\boldsymbol{k}) - \Sigma(\boldsymbol{k},\varepsilon)}, \tag{37}$$

with a (2,2) matrix self-energy $\Sigma(\boldsymbol{k},\varepsilon)$. Within a self-consistent Born approximation, the self-energy is given by

$$\Sigma(\boldsymbol{k},\varepsilon) = n_{\mathrm{i}}\int\frac{d\boldsymbol{k}'}{(2\pi)^2}u_{\mathrm{i}}(\boldsymbol{k}-\boldsymbol{k}')^2 G(\boldsymbol{k}',\varepsilon). \tag{38}$$

It is diagrammatically represented in Fig. 3(a).

The diagonal conductivity is given by the diagram shown in Fig. 3(b). Actually, we have

$$\sigma_{xx}(\varepsilon) = \frac{e^2\hbar}{2\pi}\int\frac{d\boldsymbol{k}}{(2\pi)^2}\mathrm{Re\,Tr}[v_x G(+)J_x(+-)G(-) - v_x G(+)J_x(++)G(+)], \tag{39}$$

where $v_x = \mathcal{H}_x/\hbar$, and $G(\pm) = G(\boldsymbol{k},\varepsilon\pm i0)$ and $J_x(+-) = J_x(\boldsymbol{k},\varepsilon+i0,\varepsilon-i0)$, etc., for simplicity. The current vertex satisfies a Bethe-Salpeter-type equation shown in Fig. 3(c), i.e.,

$$J_x(\boldsymbol{k},\varepsilon,\varepsilon') = v_x + n_{\mathrm{i}}\int\frac{d\boldsymbol{k}'}{(2\pi)^2}u_{\mathrm{i}}(\boldsymbol{k}-\boldsymbol{k}')^2 G(\boldsymbol{k}',\varepsilon) \times J_x(\boldsymbol{k}',\varepsilon,\varepsilon')G(\boldsymbol{k}',\varepsilon'). \tag{40}$$

The weak-field Hall conductivity due to the orbital motion is given by the diagrams shown in Figs. 4 and 5. For example, the contribution of the diagram shown in Fig. 4(a) is given by

$$H_{xy}^{(a)}(\varepsilon) = -\int\frac{d\boldsymbol{k}}{(2\pi)^2}\,\mathrm{Im\,Tr}\,G(-)J_x(-+)G(+)J_y(++) \times G(+)J_{xy}(+\,+\,-), \tag{41}$$

where we have introduced the double-vertex function $J_{xy}(+\,+\,-) = J_{xy}(\boldsymbol{k},\varepsilon+i0,\varepsilon+i0,\varepsilon-i0)$. The double-vertex function

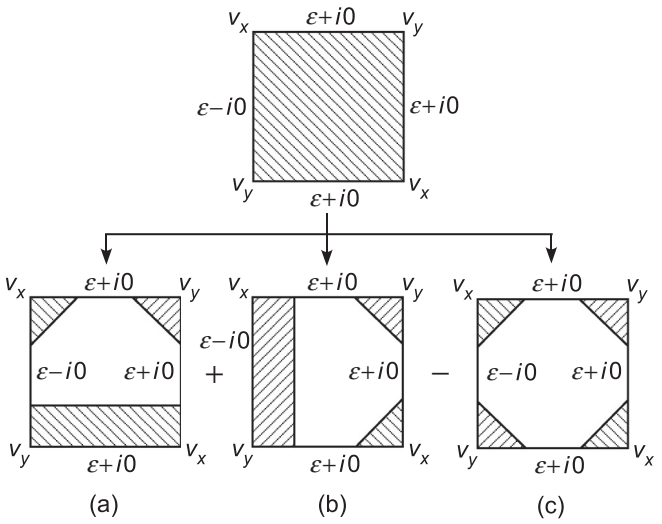

FIG. 4. The Feynman diagrams of the Hall conductivity σ'_{xy} due to the orbital motion in the self-consistent Born approximation. The term (c) appears for the purpose of removing overcounting problems.

satisfies a Bethe-Salpeter-type equation shown in Fig. 3(d), i.e.,

$$J_{xy}(\boldsymbol{k},\varepsilon,\varepsilon',\varepsilon'') = J_x(\boldsymbol{k},\varepsilon)G(\boldsymbol{k},\varepsilon')J_y(\boldsymbol{k},\varepsilon'') + n_{\rm i}\int\frac{d\boldsymbol{k}'}{(2\pi)^2}u_{\rm i}(\boldsymbol{k}-\boldsymbol{k}')^2G(\boldsymbol{k}',\varepsilon) \times J_{xy}(\boldsymbol{k}',\varepsilon,\varepsilon',\varepsilon'')G(\boldsymbol{k}',\varepsilon''). \quad (42)$$

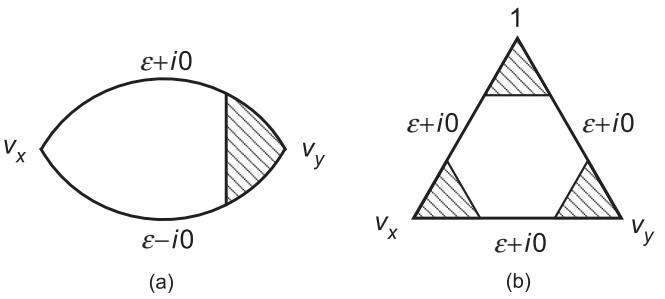

FIG. 6. The Feynman diagrams of the spin-Zeeman Hall conductivity in the self-consistent Born approximation. (a) Eq. (35). (b) Eq. (36).

All other terms are written down in the similar manner, in which vertex part J_1 and double-vertex functions such as J_{yx}, J_{1y}, etc., are introduced. Bethe-Salpeter-type equations for these additional vertex functions can be written down in a similar manner.

The spin-Zeeman Hall conductivity is given by the diagrams shown in Fig. 6. Its explicit expressions in the self-consistent Born approximation can also be written down in terms of the Green's function and vertex functions, although not shown here.

III. NUMERICAL CALCULATIONS

A. Model of dominant scatterers

For the purpose of clarifying the dependence on the potential range of dominant scatterers, we shall first con-

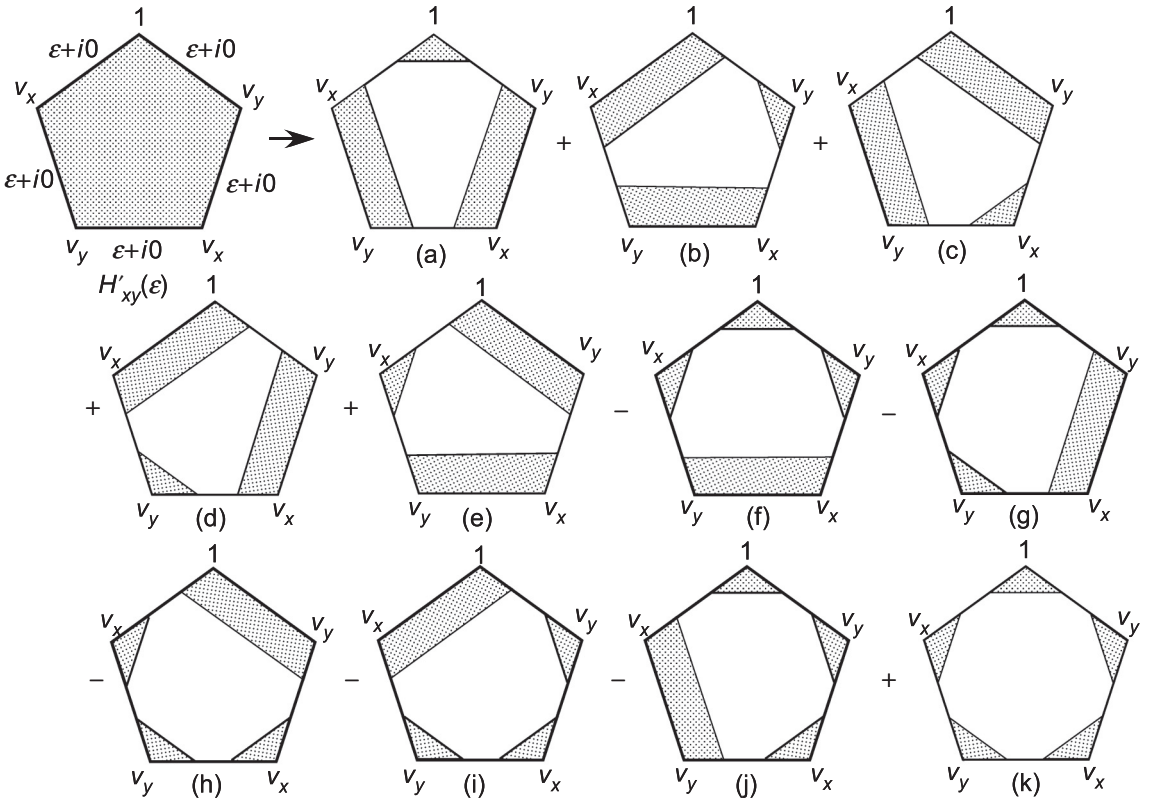

FIG. 5. The Feynman diagrams of the Hall conductivity σ''_{xy} due to the orbital motion in the self-consistent Born approximation. Terms (f)–(k) appear for the purpose of removing overcounting problems in (a)–(e).

sider scatterers with a Gaussian potential with range d and strength u,

$$u_{\rm i}(r) = \frac{u}{\pi d^2} \exp\left(- \frac{r^2}{d^2} \right). \tag{43}$$

As a more realistic source of dominant scatterers, we assume charged impurities having potential

$$u_{\rm i}(q) = \frac{2\pi e^2}{\kappa} \frac{e^{-q|z_{\rm i}|}}{q + q_{\rm s}}, \tag{44}$$

where κ is the static dielectric constant of the environment, $z_{\rm i}$ is the position of an impurity relative to the two-dimensional plane, and $q_{\rm s}$ is the Thomas-Fermi screening constant. In the following, we shall confine ourselves to the case of $z_{\rm i} = 0$ for simplicity.

The screening constant is given by $q_{\rm s} = (2\pi e^2/\kappa) D(\varepsilon_{\rm F})$ with $\varepsilon_{\rm F}$ being the Fermi energy at low temperature. In the vicinity of zero energy, the density of states is dominated by that associated with the outer band, D_+, and therefore can be approximated to be independent of energy. Thus, $q_{\rm s}$ will be regarded as an energy-independent parameter without any attempt to its self-consistent determination as was made in monolayer and bilayer graphene [49–54,86,87].

In the absence of the spin-orbit interaction, the relaxation time τ_0 and transport relaxation time τ_1 become

$$\begin{aligned} \frac{\hbar}{\tau_0(\varepsilon_k)} &= 2\pi n_{\rm i} \int \frac{d\boldsymbol{k}'}{(2\pi)^2} u_{\rm i}(\boldsymbol{k}-\boldsymbol{k}')^2 \delta(\varepsilon_k - \varepsilon_{k'}), \\ \frac{\hbar}{\tau_1(\varepsilon_k)} &= 2\pi n_{\rm i} \int \frac{d\boldsymbol{k}'}{(2\pi)^2} u_{\rm i}(\boldsymbol{k}-\boldsymbol{k}')^2 (1-\cos\theta) \delta(\varepsilon_k - \varepsilon_{k'}), \end{aligned} \tag{45}$$

where θ is the angle between $\boldsymbol{k}$ and $\boldsymbol{k}'$. In the following, the degree of disorder will be characterized by W defined in the short-range limit,

$$W = \lim_{k_{\rm so} d \to 0} \frac{\hbar}{2\tau_0(\varepsilon_{\rm so})} \frac{1}{\varepsilon_{\rm so}} = \frac{n_{\rm i} u^2 m}{2\hbar^2 \varepsilon_{\rm so}}, \tag{46}$$

for scatterers with a Gaussian potential and

$$W = \frac{n_{\rm i} m}{2\hbar^2 \varepsilon_{\rm so}} \left(\frac{2\pi e^2}{\kappa q_{\rm s}} \right)^2, \tag{47}$$

for charged impurities. In the long-range case, actual strength of the disorder cannot be characterized by the single parameter W. In fact, effects on the density of states may be characterized by $W_0 = \hbar/[2\tau_0(\varepsilon_{\rm so})\varepsilon_{\rm so}]$ and the magnitude of the conductivities may be characterized by

$$W_1 = \frac{\hbar}{2\tau_1(\varepsilon_{\rm so})} \frac{1}{\varepsilon_{\rm so}}. \tag{48}$$

These parameters for typical values of $k_{\rm so}d$ and $q_{\rm s}/k_{\rm so}$ are listed in Table I. In the following the diagonal and Hall conductivity due to orbital motion are plotted in units of quantities characterized by W_1 instead of W.

B. Boltzmann conductivities

Some examples for scatterers with a Gaussian potential are shown in Fig. 7. The diagonal conductivity shown in Fig. 7(a) exhibits a kink at $\varepsilon = 0$ when the potential range is small, i.e., $k_{\rm so}d \lesssim 1$. This structure corresponds to the linearly vanishing density of states at $\varepsilon = 0$ of the inner band, leading to the reduction of scattering of electrons in the outer band dominantly contributing to the conductivity. In fact, this kink structure disappears in the case of long-range scatterers, for which such interband scattering does not take place.

TABLE I. Some examples of W_0/W and W_1/W, characterizing the strength of disorder for (a) scatterers with a Gaussian potential and (b) charged impurities.

	(a)	
$k_{\rm so}d$	W_0/W	W_1/W
0.2	0.961	0.942
0.5	0.791	0.693
1.0	0.466	0.258
1.5	0.287	0.076
2.0	0.207	0.028
	(b)	
$q_{\rm s}/k_{\rm so}$	W_0/W	W_1/W
10.0	0.794	0.7328
2.0	0.424	0.3023
0.5	0.147	0.0586
0.1	0.032	0.0040

The Hall conductivity shown in Fig. 7(b) exhibits a discrete jump at $\varepsilon = 0$ and the jump height seems to increase with

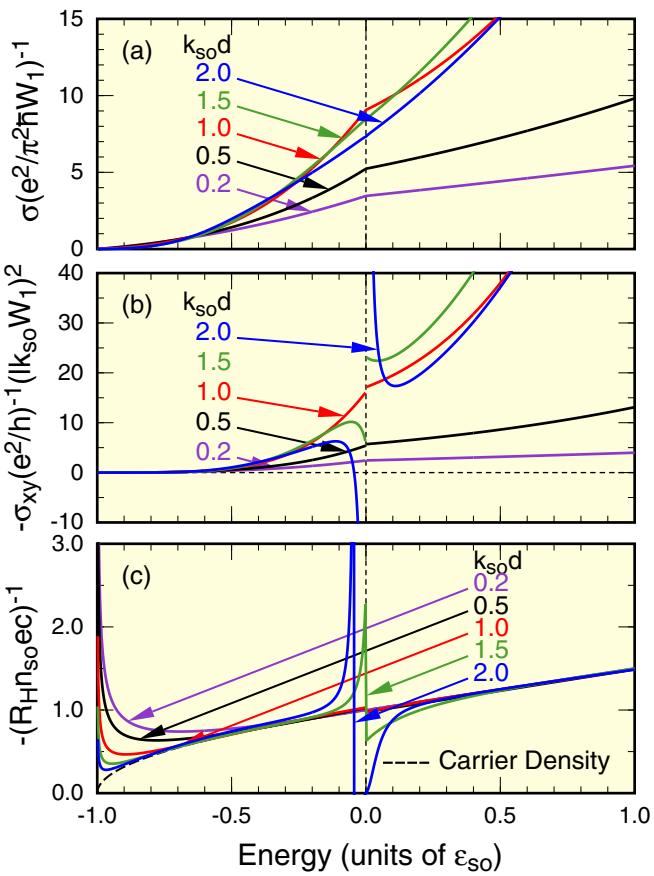

FIG. 7. Some examples of the (a) diagonal conductivity, (b) Hall conductivity, and (c) inverse Hall coefficient for scatterers with a Gaussian potential with range d, obtained in the Boltzmann transport theory.

the potential range. For sufficiently large potential range such as $k_{so}d = 2$, σ_{xy} exhibits very singular behavior and even a sign change. This corresponds to the similar singular behavior appearing in monolayer graphene having a single Weyl cone [38,54]. In fact, in the case of long-range scatterers, two bands with large and small wave vectors, k_+ and k_-, become almost independent of each other, making the singular behavior in the Weyl system apparent. This singularity appears also in the Hall coefficient shown in Fig. 7(c).

The Hall conductivity shown in Fig. 7(b) rapidly decreases with decreasing energy below $\varepsilon = 0$ and becomes vanishingly small when the energy approaches the band bottom $-\varepsilon_{so}$. The reason lies in the cancellation of the contribution of the two bands with k_+ and k_-. The latter band, having a negative cyclotron frequency and behaving as a hole band, tends to cancel the Hall conductivity of the k_+ band. In the vicinity of the band bottom, the cancellation is expected to become exact.

This cancellation due to the electronlike and holelike bands manifests itself as the increase of the inverse Hall coefficient, R_H^{-1}, in the low-energy region $\varepsilon < -\varepsilon_{so}/2$ in Fig. 7(c). In the vicinity of the band bottom $\varepsilon = -\varepsilon_{so}$, R_H^{-1} exhibits singular and divergent behavior. Near zero energy, R_H^{-1} exhibits a discrete jump and its amount increases with the potential range. In the case of long-range scatterers like $k_{so}d = 2$, R_H^{-1} exhibits divergence near zero energy corresponding to the sign change in σ_{xy}.

Some examples of the Boltzmann results for charged impurities with $z_i = 0$ are shown in Fig. 8. The most striking difference between charged impurities and scatterers with a Gaussian potential becomes apparent in the long-range case $q_s \ll k_{so}$. In fact, no singular behavior at $\varepsilon = 0$ manifests itself in Fig. 8(b) σ_{xy} and Fig. 8(c) R_H^{-1} even in the case of very small screening constant. This is presumably due to the fact that interband scattering remains appreciable even in this case and the real singular behaviors associated with the zero-mass Dirac bands are washed out. Persistent interband effects also cause the appearance of a kinklike structure in the diagonal conductivity shown in Fig. 8(a) even for $q_s/k_{so} = 0.1$. The reduction of the Hall conductivity due to the cancellation between the electronlike and holelike bands in the low-energy region $\varepsilon < -\varepsilon_{so}/2$ occurs independent of kinds of scatterers as shown in Figs. 8(b) and 8(c).

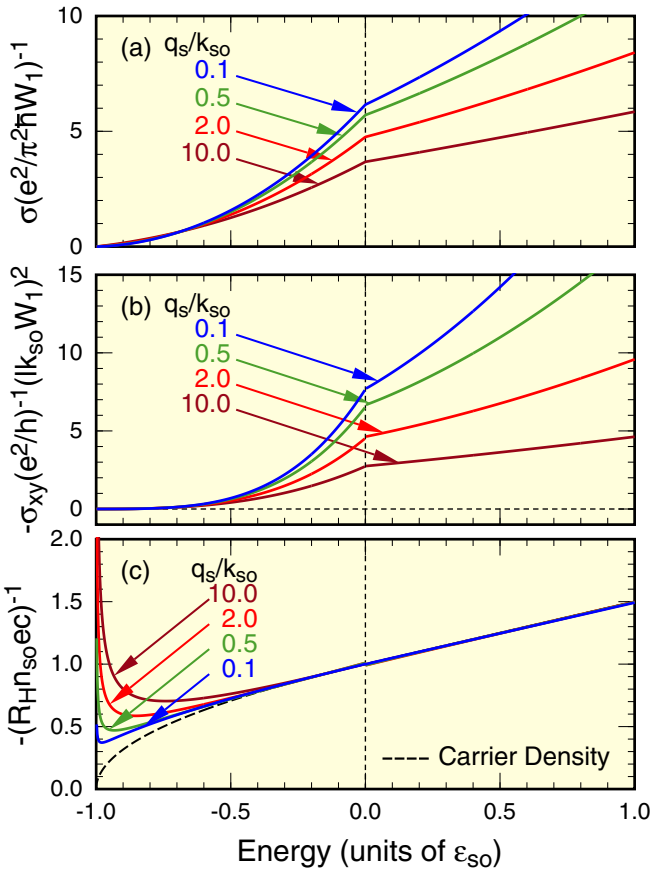

FIG. 8. Some examples of the (a) diagonal conductivity, (b) Hall conductivity, and (c) inverse Hall coefficient for dominant charged-impurity scattering with screening constant q_s, obtained in the Boltzmann transport theory.

C. Self-consistent Born approximation

The dependence of the Green's function, the self-energy, and the vertex functions on the direction angle $\theta_{\boldsymbol{k}}$ of $\boldsymbol{k}$ can be eliminated as has previously been discussed [49–54]. Then, the self-consistency equation for the self-energy and the Bethe-Salpeter-type equations for the vertex functions are all solved iteratively by discretization of k. For actual calculations, we introduce cutoff energy ε_c and wave vector k_c through $\varepsilon_c = \hbar^2 k_c^2/(2m)$. We choose $k_{so}/k_c = 0.1$ and therefore $\varepsilon_{so}/\varepsilon_c = 0.01$, and we discretize the wave vector such that

$$k_j = \frac{1}{2}\Delta k_j + \sum_{j'=1}^{j-1} \Delta k_{j'} \quad (j = 1, \ldots, j_{max}),$$
$$\sum_{j=1}^{j_{max}} \Delta k_j = k_c. \tag{49}$$

Then, we can make the following replacement:

$$\int_0^{k_c} k dk\, F(k) \Rightarrow \sum_{j=1}^{j_{max}} \Delta k_j\, k_j\, F(k_j). \tag{50}$$

Furthermore, we use $\Delta k_j \propto (j+\alpha)^\beta$ with $\alpha \approx 0$ and $\beta \approx 1$. We shall choose $j_{max} = 1000 \sim 2000$ depending on actual values of the imaginary part of the self-energy.

Some examples of numerical results of the density of states $D(\varepsilon)$ and the electron density n_s for scatterers with a Gaussian potential are shown in Fig. 9. In the case of short-range scatterers $k_{so}d = 0.2$ shown in Fig. 9(a), the density of states has a peak around $\varepsilon \approx -\varepsilon_{so}$ almost independent of disorder parameter W. In the long-range case $k_{so}d = 2$, on the other hand, the peak energy is shifted to higher-energy side with W. This is presumably due to the fact that states are pushed toward the low-energy side due to quantum mechanical repulsion with higher-energy states in the short-range case, while in the long-range case, effects of impurity potential rapidly become weaker with energy and effects of downward level-shift are weaker than those of upward shift. The resulting enhancement of the density of states near zero energy tends to reduce the diagonal and Hall conductivity as will be discussed below.

Figure 10 shows calculated Fig. 10(a) σ_{xx}, Fig. 10(b) σ_{xy}, and Fig. 10(c) R_H^{-1} in the short-range case of $k_{so}d = 0.2$.

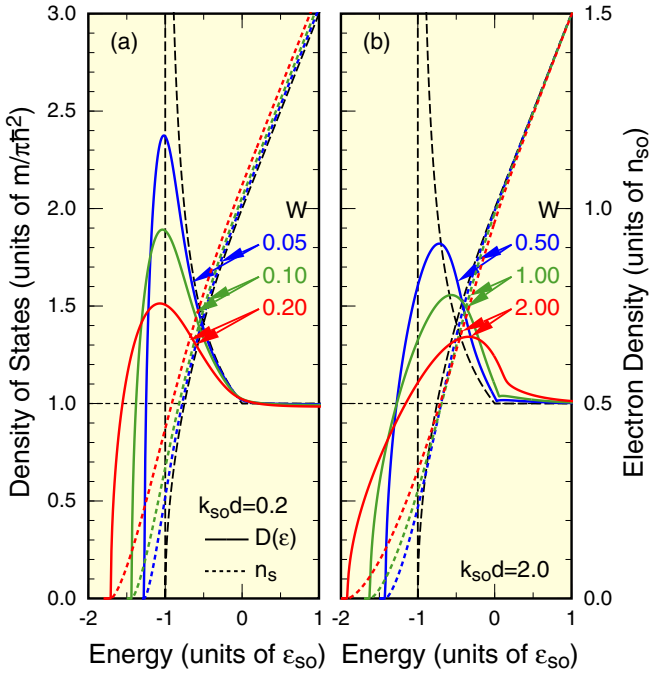

FIG. 9. Some examples of the density of states and the electron density for scatterers with a Gaussian potential, calculated in the self-consistent Born approximation. (a) $k_{so}d = 0.2$ (short range) and (b) 2 (long range).

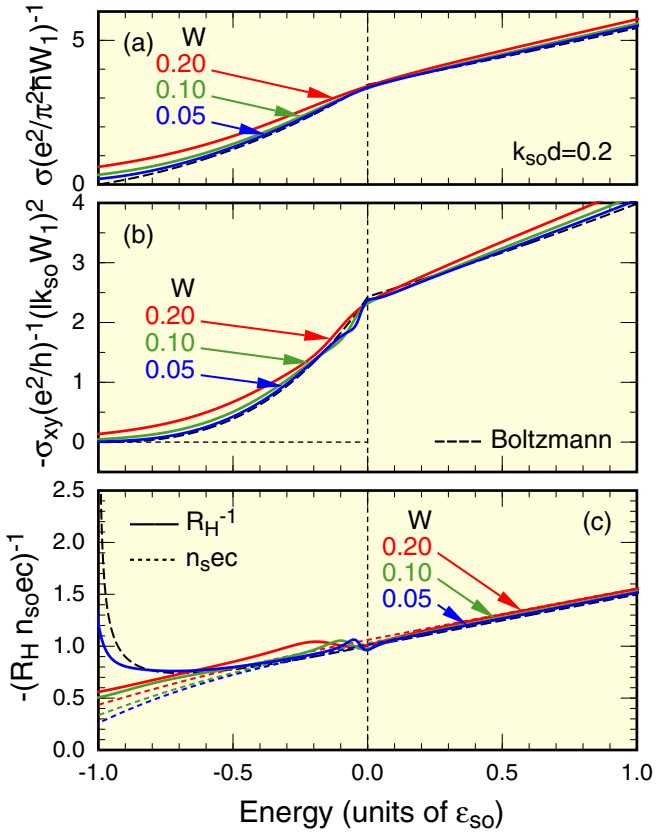

FIG. 10. Some examples of the (a) diagonal conductivity, (b) Hall conductivity, and (c) inverse Hall coefficient for scatterers with a Gaussian potential, calculated in the self-consistent Born approximation. $k_{so}d = 0.2$ (short range).

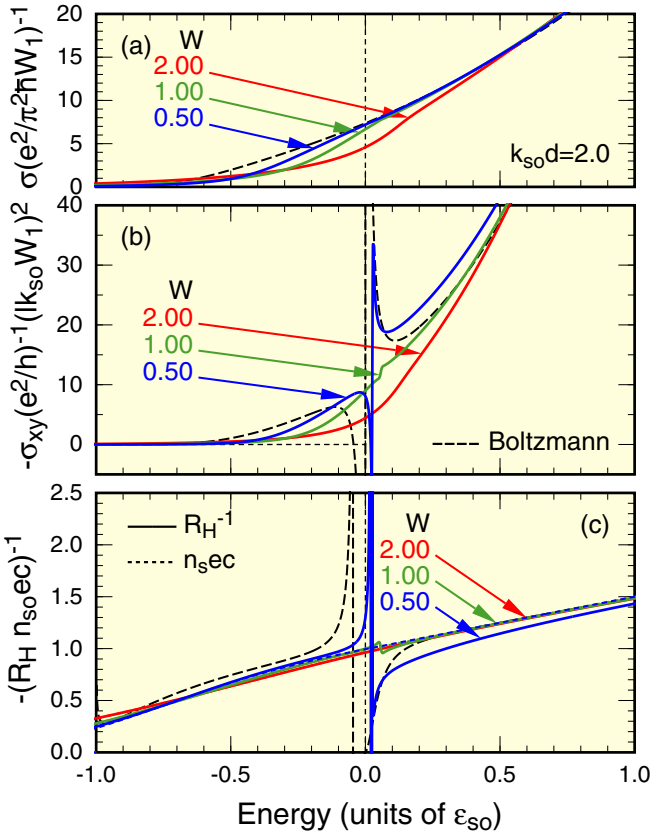

FIG. 11. Some examples of the (a) diagonal conductivity, (b) Hall conductivity, and (c) inverse Hall coefficient for scatterers with a Gaussian potential, calculated in the self-consistent Born approximation. $k_{so}d = 2$ (long range).

The diagonal conductivity is close to the Boltzmann result and does not exhibit singular drop at $\varepsilon = 0$ as in monolayer graphene [27,49]. This is due to the fact that induced current is dominated by electrons belonging to the outer band. The Hall conductivity exhibits a steplike change near $\varepsilon = 0$, giving rise to a step structure in the inverse Hall coefficient. Such a structure does not vanish even in the case of large disorder $W = 0.2$. This step structure looks close to that in the results obtained by assuming an energy-independent broadening in monolayer graphene [41,42]. This may be reasonable because the presence of the outer band with large density of states dominantly causes energy-independent broadening of the inner band.

Figure 11 shows the corresponding results in the long-range case ($k_{so}d = 2$). The singular jump at $\varepsilon = 0$ of σ_{xy} is very sensitive to the degree of disorder W. For small disorder $W \lesssim 0.5$ both σ_{xy} and R_H^{-1} exhibit qualitatively the same behavior as the Boltzmann result, while for large disorder $W \gtrsim 1$, only a small step remains or the jump completely disappears. For the largest disorder $W = 2$, both σ_{xx} and σ_{xy} are reduced considerably from the corresponding Boltzmann results near zero energy. This can be understood as results of considerable mixing of low-energy states contributing less to the current, corresponding to enhanced density of states shown in Fig. 9(b).

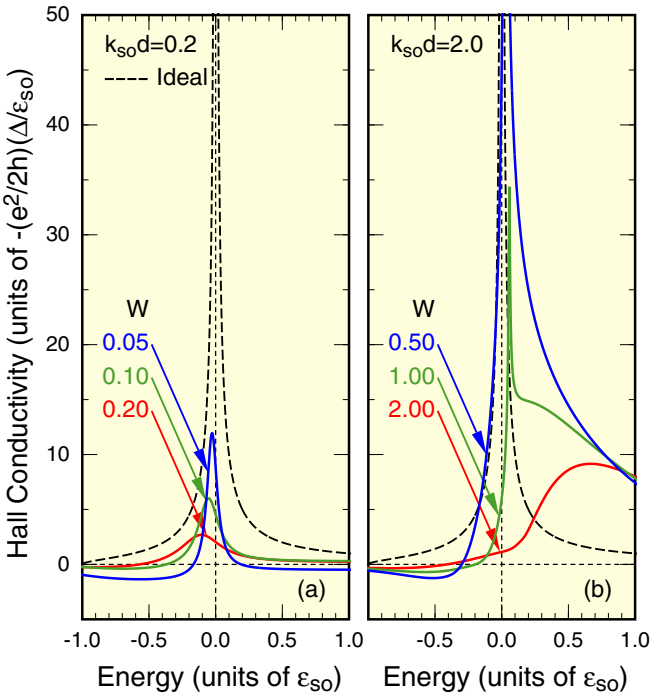

FIG. 12. Some examples of the spin-Zeeman Hall conductivity for scatterers with a Gaussian potential, calculated in the self-consistent Born approximation. (a) $k_{so}d = 0.2$ (short range) and (b) 2 (long range).

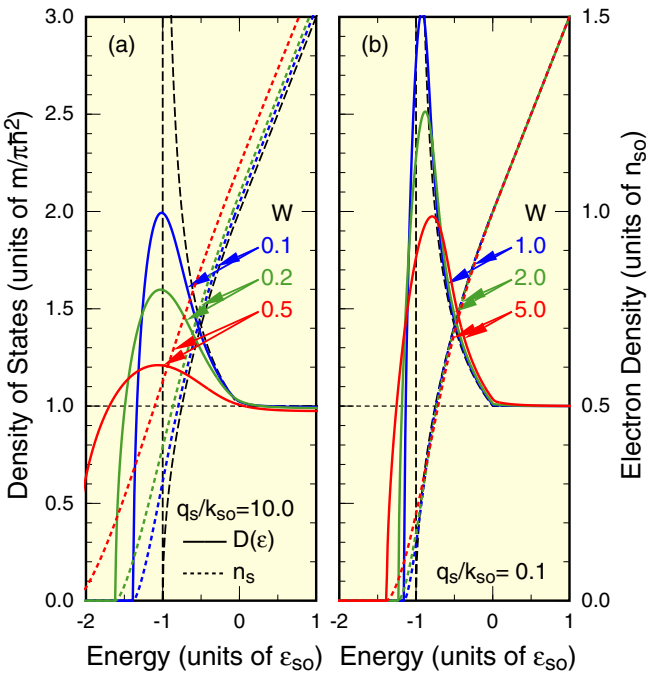

FIG. 13. Some examples of the density of states and the electron density for charged-impurity scattering, calculated in the self-consistent Born approximation. (a) $q_s/k_{so} = 10$ (short range) and (b) 0.1 (long range).

Figure 12 shows the spin-Zeeman Hall conductivity in the case of very small gap $\Delta/\varepsilon_{so} = 0.01$. The conductivity is proportional to the gap for this Δ and can be regarded as the contribution of the spin-Zeeman effect to the weak-field Hall conductivity, when we set $\Delta = \frac{1}{2}g\mu_B B$. In the short-range case $k_{so}d = 0.2$ shown in Fig. 12(a), the spin-Zeeman Hall conductivity is reduced considerably from the ideal result. This shows clearly that mixing of the inner band with the outer band tends to destroy the spin-Zeeman effect.

In the long-range case $k_{so}d = 2$, the conductivity becomes comparable to or larger than the ideal result. In fact, in the energy region $\varepsilon > 0$ ($k_F d \gg 1$ with k_F the Fermi wave vector) where interband mixing may be almost completely neglected, it is much enhanced from the ideal result. This enhancement corresponds to the similar behavior in the valley Hall conductivity in graphene [52,53], as will be discussed in Sec. IV. In the low-energy region $\varepsilon < 0$, the conductivity is reduced and even changes the sign with the decrease of ε, because d becomes smaller than k_F^{-1} there, causing the increase of interband mixing.

Figures 13 shows some examples of the density of states and the electron density in the case of dominant charged-impurity scattering. Its qualitative behavior, in particular, the dependence on W and q_s/k_{so}, is similar to that in the case of scatterers with a short-range Gaussian potential shown in Fig. 9. No enhancement of the density of states near zero energy appears even for $q_s/k_{so} = 0.1$.

The corresponding results for the transport quantities are given in Figs. 14 and 15. Qualitatively, the behavior of the diagonal conductivity is almost independent of q_s/k_{so} in contrast to the case of scatterers with a Gaussian potential

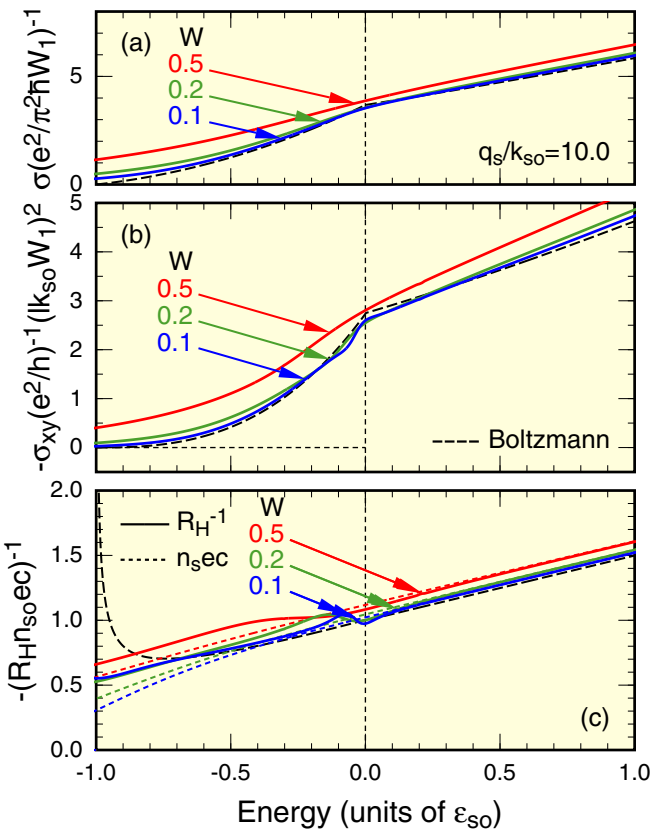

FIG. 14. Some examples of the (a) diagonal conductivity, (b) Hall conductivity, and (c) inverse Hall coefficient for dominant charged-impurity scattering, calculated in the self-consistent Born approximation. $q_s/k_{so} = 10$ (short range).

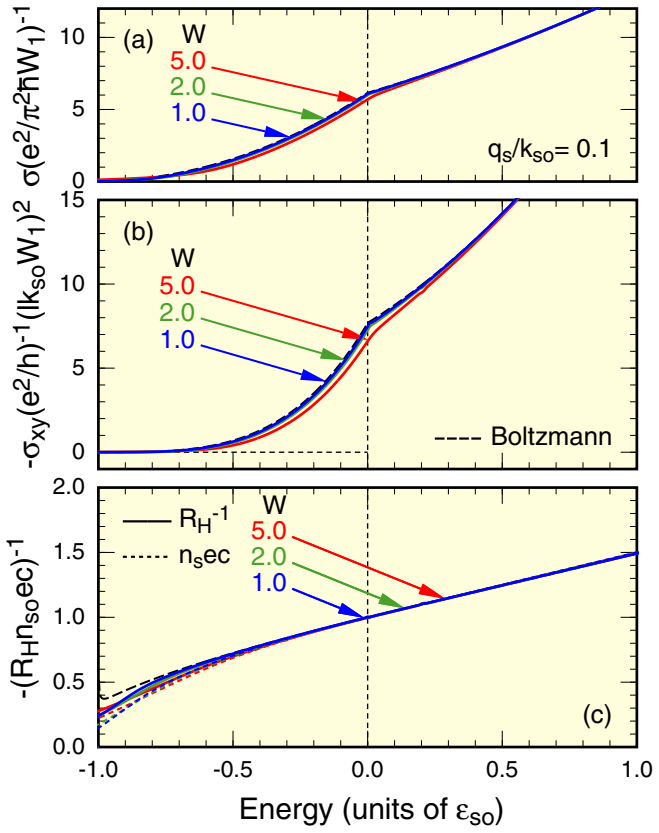

FIG. 15. Some examples of the (a) diagonal conductivity, (b) Hall conductivity, and (c) inverse Hall coefficient for dominant charged-impurity scattering, calculated in the self-consistent Born approximation. $q_s/k_{so} = 0.1$ (long range).

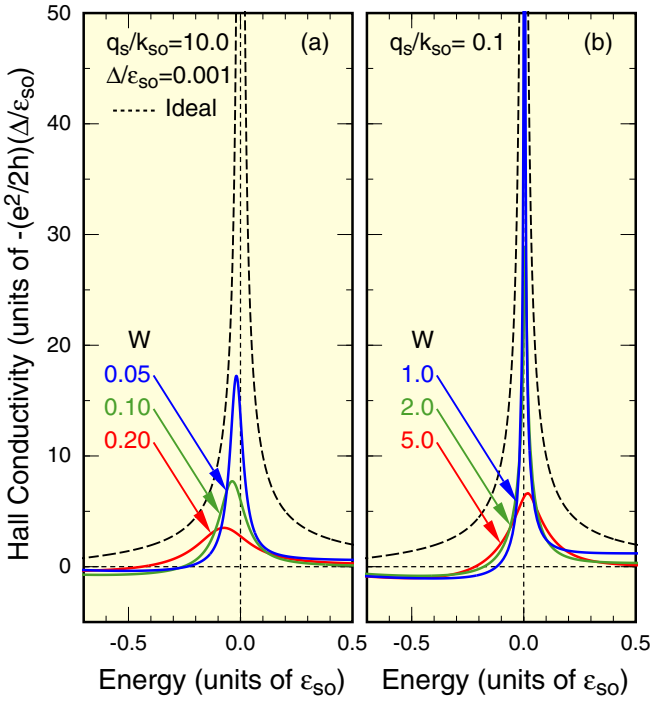

FIG. 16. Some examples of the spin-Zeeman Hall conductivity for charged-impurity scattering, calculated in the self-consistent Born approximation. (a) $q_s/k_{so} = 10$ (short range) and (b) 0.1 (long range).

shown in Figs. 10(a) and 11(a), and no significant reduction occurs near zero energy even for large W.

In the short-range case shown in Figs. 14(b) and 14(c), the Hall conductivity exhibits a clear steplike feature near $\varepsilon = 0$, causing an associated feature in the Hall coefficient, in agreement with the behavior for scatterers with a Gaussian potential shown in Figs. 10(b) and 10(c). In the long-range case shown in Fig. 15(b), the Hall conductivity does not exhibit any singular behavior in contrast to the case of scatterers with a Gaussian potential and is close to the Boltzmann result. Correspondingly, the Hall coefficient varies smoothly across $\varepsilon = 0$ as the Boltzmann result. This shows again that interband mixing effects remain important for the Coulomb potential independent of the amount of screening.

Figure 16 shows some examples of the spin-Zeeman Hall conductivity in the case of charged impurities. In the short-range case shown in Fig. 16(a), the conductivity is in semiquantitative agreement with that for scatterers with a Gaussian potential shown in Fig. 12(a). In the long-range case shown in Fig. 16(b), however, the conductivity remains much smaller than the ideal result and the prominent asymmetry in Fig. 12(b) does not appear. This again shows the presence of appreciable amount of interband mixing, reducing the spin-Zeeman Hall conductivity.

IV. DISCUSSION

When we take the limit of $k_{so} \to \infty$ and $m \to \infty$ for fixed $\gamma \equiv \hbar^2 k_{so}/m$ and rotate $\hat{\boldsymbol{k}}$ by $\pi/2$, the Hamiltonian becomes the same as that of electrons in the vicinity of a K point in the first Brillouin zone of graphene, where a gap is induced by asymmetry in the energy of two sublattice points. By taking the limit $\varepsilon_{so} \to \infty$ in Eq. (21), the spin-Zeeman Hall conductivity is quantized into $\pm e^2/(2h)$ in the gap [19,88–91], and its absolute value monotonically decreases in the band continuum [92,93]. This is the same as the valley Hall conductivity in ideal graphene with gap. Because induced current is canceled by that of a K' point, no Hall voltage appears, but the presence of the valley Hall effect has been experimentally confirmed using a nonlocal resistance in both monolayer [94] and bilayer graphene [95,96].

Detailed study of disorder effects on the valley Hall conductivity in graphene was performed recently [52,53]. The result shows that in the presence of scatterers, the valley Hall conductivity in the band continuum is strongly enhanced and that this enhancement depends on the explicit form of scattering potential even in the clean limit, where the concentration and strength of scatterers are vanishingly small. The result for short-range scatterers in the clean limit agrees with that previously obtained [97]. Furthermore, numerical calculations in the self-consistent Born approximation shows that the valley Hall conductivity remains appreciable because of the enhancement even in the case of large disorder.

Figure 17 shows some examples for this single Weyl system with scatterers with a Gaussian potential with range d. In the small-gap limit corresponding to the spin-Zeeman Hall conductivity, the result becomes universal when the

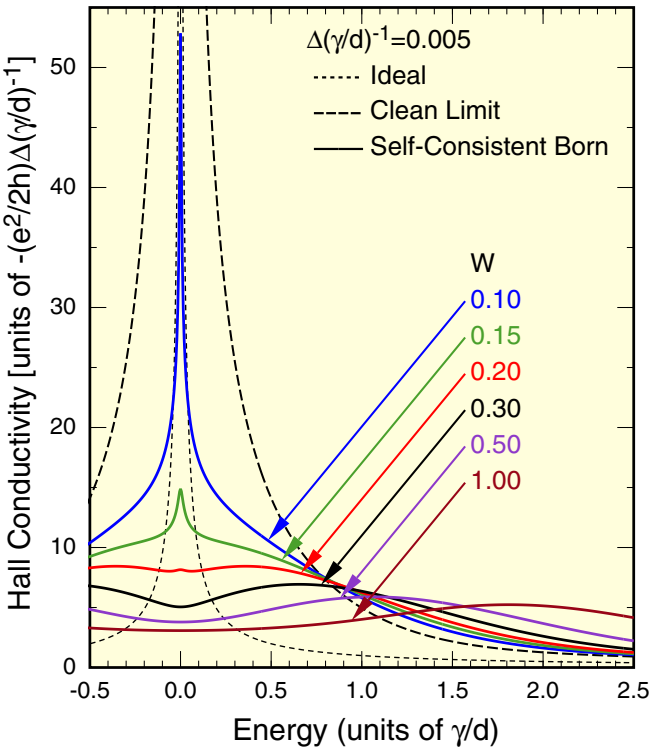

FIG. 17. Some examples of the spin-Zeeman Hall conductivity for scatterers with a Gaussian potential in a single Weyl system.

energy is scaled by γ/d. The disorder parameter is defined by $W = n_i u^2/(4\pi\gamma^2)$ following the conventions in graphene [27,36–38,49–54]. The singular behavior $\propto |\varepsilon|^{-1}$ near zero energy is considerably reduced and easily smoothed out by disorder, but the conductivity in the other region is enhanced over the ideal result and can be even larger than the clean-limit result away from zero energy.

In the present system, however, a similar enhancement appears only in the high-energy region of Fig, 12(b), where the inner and outer bands are regarded as almost independent, and does not in Fig. 12(a) and in Fig. 16, for which mixing between the inner and outer bands cannot be neglected. This clearly shows that the important feature in the Weyl system is easily destroyed by small mixing with the outer band and therefore may hardly manifest itself in the Rashba system.

In order to discuss relative importance of the orbital-motion and the spin-Zeeman contributions to the Hall conductivity, let us first consider the case of short-range scatterers. The orbital Hall conductivity $\sigma_{xy}^{\rm orb}$ is roughly of the order of $(e^2/h) \times (lk_{\rm so}W)^{-2}$ and the spin-Zeeman conductivity $\sigma_{xy}^{\rm spin}$ is roughly $(e^2/h) \times (g\mu_{\rm B}B)/(2\varepsilon_{\rm so}W)$, giving $\sigma_{xy}^{\rm spin}/\sigma_{xy}^{\rm orb} \sim \tilde{g}W$, with

$$\tilde{g} = \frac{g}{2}\frac{m}{m_0}. \tag{51}$$

The actual numerical results presented in the previous section show that the spin-Zeeman conductivity is considerably reduced from the above due to mixing between the inner and outer bands. Then, we have $\sigma_{xy}^{\rm spin}/\sigma_{xy}^{\rm orb} \ll \tilde{g}W$.

In conventional III-V and II-VI semiconductors, the bottom of the conduction band consists of s-like orbitals $|s)$ and the top of the valence bands p-like orbitals $|x)$, $|y)$, and $|z)$. When only these bands are considered, the effective mass and the g factor of the conduction-band bottom are given by [98–100]

$$\frac{m_0}{m} = 1 + \frac{1}{3}\frac{\varepsilon_P}{\varepsilon_G}\frac{3\varepsilon_G + 2\Delta_{\rm so}}{\varepsilon_G + \Delta_{\rm so}}, \tag{52}$$

$$g = 2 - \frac{2}{3}\frac{\varepsilon_P}{\varepsilon_G}\frac{\Delta_{\rm so}}{\varepsilon_G + \Delta_{\rm so}}, \tag{53}$$

with ε_G being the band gap, $\Delta_{\rm so}$ the spin-orbit splitting in the valence band, and $\varepsilon_P = P^2/2m_0$, where P represents an interband matrix element of momentum, i.e., $P = -i(s|p_z|z)$. Actually, the presence of other bands should be considered except in narrow-gap semiconductors, giving corrections to the above formula [101–105], but the qualitative dependence on $\Delta_{\rm so}$ and ε_G remains essentially unaffected.

This gives

$$-\frac{1}{2} < \tilde{g} < \left(1 + \frac{\varepsilon_P}{\varepsilon_G}\right)^{-1}. \tag{54}$$

Usually, $\varepsilon_P \sim 20$ eV and $\varepsilon_G \lesssim 1$ eV, we have $\tilde{g} \ll 1$ when $\tilde{g} > 0$. Therefore, the spin-Zeeman contribution becomes observable only in very dirty systems $W \gtrsim 0.5$, for which the peak structure is almost completely smoothed out. In the case of long-range scatterers, $\sigma_{xy}^{\rm orb} \propto (W/W_1)^2$ becomes much larger than the above estimate because of the renormalization of the transport relaxation time, i.e., $W_1 \ll W$, while no significant enhancement is present for $\sigma_{xy}^{\rm spin}$. As a result, $\sigma_{xy}^{\rm spin}/\sigma_{xy}^{\rm orb}$ is further reduced. Therefore, the spin-Zeeman Hall conductivity remains in general much smaller than the orbital Hall conductivity in the present system.

Finally, we give several comments from the viewpoint of the anomalous Hall effect. The system with nonzero Δ due to magnetization or an exchange field has nonzero Hall conductivity even in the absence of magnetic field. The spin-Zeeman contribution $\sigma_{xy}^{\rm spin}$ in this study corresponds to this anomalous Hall conductivity. There have been a great number of investigations on several types of contributions, which are described by the intrinsic contribution, the side-jump effect, and the skew scattering in the semiclassical transport theory. The first and second contributions are fully taken into consideration in the present study, while the third is not [63].

In the self-consistent Born approximation, we consider the case of high concentrations of weak scatterers where multiple scattering by a single impurity does not play significant roles. On the other hand, the skew scattering arises when we include effects of higher-order scattering processes by a single impurity. It can give a dominant contribution to the anomalous Hall conductivity as has been demonstrated by calculations in a self-consistent T-matrix approximation [62,70]. Evaluation of such higher-order effects on transport properties in the present giant Rashba system, including the weak-field Hall effect, could be an important task in the near future.

Recently, it has been pointed out that diagrams with a single pair of crossing impurity-scattering lines give additional contributions to the anomalous Hall conductivity comparable to those of the intrinsic and side-jump mechanisms [81,82]. Certainly, such effects, not included in the self-consistent Born approximation, can give some corrections to $\sigma_{xy}^{\rm spin}$. As shown in the preceding discussions, however, the Hall effect in the

present system is dominated by the orbital contribution given by $\sigma_{xy}^{\rm orb}$ except in quite dirty cases.

V. SUMMARY

In summary, we have calculated the weak-field Hall conductivity of a two-dimensional system with a strong Rashba spin-orbit interaction containing scatterers with long-range potential such as those with a Gaussian potential and charged impurities. The Hall conductivity consists of two contributions due to orbital cyclotron motion and spin-Zeeman splitting corresponding to the spin-Zeeman Hall conductivity. The singular behavior of the orbital Hall conductivity associated with the band crossing at $\boldsymbol{k} = 0$, which appears only in the long-range case of scatterers with a Gaussian potential, disappears in the presence of small interband mixing. The spin-Zeeman Hall conductivity is considerably reduced due to interband mixing and its significant enhancement due to scattering for the single Weyl system as in graphene does not take place in the present system. Except in very dirty cases, the spin-Zeeman term does not give appreciable contribution to the Hall conductivity.

ACKNOWLEDGMENTS

This work has been supported in part by MEXT (Japan) Grants-in-Aid for Scientific Research on Innovative Areas "Science of Atomic Layers" (Project No. 2506) and Scientific Research (Projects No. 24540339, No. 25400313, and No. 16K05391).

[1] G. Bihlmayer, O. Rader, and R. Winkler, New J. Phys. **17**, 050202 (2015).
[2] I. Zutic, J. Fabian, and S. Das Sarma, Rev. Mod. Phys. **76**, 323 (2004).
[3] P. D. C. King, R. C. Hatch, M. Bianchi, R. Ovsyannikov, C. Lupulescu, G. Landolt, B. Slomski, J. H. Dil, D. Guan, J. L. Mi, E. D. L. Rienks, J. Fink, A. Lindblad, S. Svensson, S. Bao, G. Balakrishnan, B. B. Iversen, J. Osterwalder, W. Eberhardt, F. Baumberger, and Ph. Hofmann, Phys. Rev. Lett. **107**, 096802 (2011).
[4] K. Ishizaka, M. S. Bahramy, H. Murakawa, M. Sakano, T. Shimojima, T. Sonobe, K. Koizumi, S. Shin, H. Miyahara, A. Kimura, K. Miyamoto, T. Okuda, H. Namatame, M. Taniguchi, R. Arita, N. Nagaosa, K. Kobayashi, Y. Murakami, R. Kumai, Y. Kaneko, Y. Onose, and Y. Tokura, Nature Mater. **10**, 521 (2011).
[5] G.-H. Lee, Y.-J. Yu, C.-G. Lee, C. Dean, K. L. Shepard, P. Kim, and J. Hone, Appl. Phys. Lett. **99**, 243114 (2011).
[6] L. Demkó, G. A. H. Schober, V. Kocsis, M. S. Bahramy, H. Murakawa, J. S. Lee, I. Kezsmarki, R. Arita, N. Nagaosa, and Y. Tokura, Phys. Rev. Lett. **109**, 167401 (2012).
[7] M. Sakano, J. Miyawaki, A. Chainani, Y. Takata, T. Sonobe, T. Shimojima, M. Oura, S. Shin, M. S. Bahramy, R. Arita, N. Nagaosa, H. Murakawa, Y. Kaneko, Y. Tokura, and K. Ishizaka, Phys. Rev. B **86**, 085204 (2012).
[8] S. Bordacs, J. G. Checkelsky, H. Murakawa, H. Y. Hwang, and Y. Tokura, Phys. Rev. Lett. **111**, 166403 (2013).
[9] H. Murakawa, M. S. Bahramy, M. Tokunaga, Y. Kohama, C. Bell, Y. Kaneko, N. Nagaosa, H. Y. Hwang, and Y. Tokura, Science **342**, 1490 (2013).
[10] L. Ye, J. G. Checkelsky, F. Kagawa, and Y. Tokura, Phys. Rev. B **91**, 201104 (2015).
[11] G. A. H. Schober, H. Murakawa, M. S. Bahramy, R. Arita, Y. Kaneko, Y. Tokura, and N. Nagaosa, Phys. Rev. Lett. **108**, 247208 (2012).
[12] M. Sakano, M. S. Bahramy, A. Katayama, T. Shimojima, H. Murakawa, Y. Kaneko, W. Malaeb, S. Shin, K. Ono, H. Kumigashira, R. Arita, N. Nagaosa, H. Y. Hwang, Y. Tokura, and K. Ishizaka, Phys. Rev. Lett. **110**, 107204 (2013).
[13] E. I. Rashba, Fizika tverd. tela, **1**, 407 (1959) [Sov. Phys. Solid State **1**, 368 (1959)].
[14] E. I. Rashba, Fizika tverd. tela, **2**, 1224 (1960) [Sov. Phys. Solid State **2**, 1109 (1960)].
[15] Yu. A. Bychkov and E. I. Rashba, J. Phys. C **17**, 6039 (1984).
[16] J. W. McClure, Phys. Rev. **104**, 666 (1956).
[17] J. C. Slonczewski and P. R. Weiss, Phys. Rev. **109**, 272 (1958).
[18] D. P. DiVincenzo and E. J. Mele, Phys. Rev. B **29**, 1685 (1984).
[19] G. W. Semenoff, Phys. Rev. Lett. **53**, 2449 (1984).
[20] H. Ajiki and T. Ando, J. Phys. Soc. Jpn. **62**, 1255 (1993).
[21] C. L. Kane and E. J. Mele, Phys. Rev. Lett. **78**, 1932 (1997).
[22] T. Ando, J. Phys. Soc. Jpn. **74**, 777 (2005).
[23] T. Ando, Physica E **40**, 213 (2007).
[24] A. H. Castro Neto, F. Guinea, N. M. Peres, K. S. Novoselov, and A. K. Geim, Rev. Mod. Phys. **81**, 109 (2009).
[25] D. S. L. Abergel, V. Apalkov, J. Berashevich, K. Ziegler, and T. Chakraborty, Adv. Phys. **59**, 261 (2010).
[26] T. Ando, J. Appl. Phys. **109**, 102401 (2011).
[27] N. H. Shon and T. Ando, J. Phys. Soc. Jpn. **67**, 2421 (1998).
[28] A. K. Geim and K. S. Novoselov, Nature Mater. **6**, 183 (2007).
[29] S. A. Safran and F. J. DiSalvo, Phys. Rev. B **20**, 4889 (1979).
[30] M. Koshino, Y. Arimura, and T. Ando, Phys. Rev. Lett. **102**, 177203 (2009).
[31] M. Koshino and T. Ando, Phys. Rev. B **81**, 195431 (2010).
[32] M. Koshino and T. Ando, Solid State Commun. **151**, 1054 (2011).
[33] T. Ando and T. Nakanishi, J. Phys. Soc. Jpn. **67**, 1704 (1998).
[34] T. Ando, T. Nakanishi, and R. Saito, J. Phys. Soc. Jpn. **67**, 2857 (1998).
[35] T. Ando and H. Suzuura, J. Phys. Soc. Jpn. **71**, 2753 (2002).
[36] Y. Zheng and T. Ando, Phys. Rev. B **65**, 245420 (2002).
[37] T. Ando, Y. Zheng, and H. Suzuura, J. Phys. Soc. Jpn. **71**, 1318 (2002).
[38] T. Fukuzawa, M. Koshino, and T. Ando, J. Phys. Soc. Jpn. **78**, 094714 (2009).
[39] V. P. Gusynin and S. G. Sharapov, Phys. Rev. Lett. **95**, 146801 (2005).
[40] V. P. Gusynin and S. G. Sharapov, Phys. Rev. B **73**, 245411 (2006).
[41] H. Fukuyama, J. Phys. Soc. Jpn. **76**, 043711 (2007).
[42] M. Nakamura, Phys. Rev. B **76**, 113301 (2007).
[43] M. Koshino and T. Ando, Phys. Rev. B **75**, 235333 (2007).

[44] Y. Arimura, M. Koshino, and T. Ando, J. Phys. Soc. Jpn. **80**, 114705 (2011).
[45] Y. Arimura and T. Ando, J. Phys. Soc. Jpn. **81**, 024702 (2012).
[46] X.-Z. Yan, Y. Romiah, and C. S. Ting, Phys. Rev. B **77**, 125409 (2008).
[47] X.-Z. Yan and C. S. Ting, Phys. Rev. B **80**, 155423 (2009).
[48] X.-Z. Yan and C. S. Ting, New J. Phys. **11**, 093026 (2009).
[49] M. Noro, M. Koshino, and T. Ando, J. Phys. Soc. Jpn. **79**, 094713 (2010).
[50] M. Noro, M. Koshino, and T. Ando, J. Phys. Soc. Jpn. **80**, 114701 (2011).
[51] T. Ando, Physica E **58**, 6 (2014).
[52] T. Ando, J. Phys. Soc. Jpn. **84**, 114705 (2015).
[53] T. Ando, J. Phys. Soc. Jpn. **84**, 114704 (2015).
[54] M. Noro and T. Ando, J. Phys. Soc. Jpn. **85**, 014708 (2016).
[55] A. Crepieux and P. Bruno, Phys. Rev. B **64**, 014416 (2001).
[56] D. Culcer, A. H. MacDonald, and Q. Niu, Phys. Rev. B **68**, 045327 (2003).
[57] A. A. Burkov, A. S. Nunez, and A. H. MacDonald, Phys. Rev. B **70**, 155308 (2004).
[58] V. K. Dugaev, P. Bruno, M. Taillefumier, B. Canals, and C. Lacroix, Phys. Rev. B **71**, 224423 (2005).
[59] P. L. Krotkov and S. Das Sarma, Phys. Rev. B **73**, 195307 (2006).
[60] P. Kleinert and V. V. Bryksin, Solid State Commun. **139**, 205 (2006).
[61] J. I. Inoue, T. Kato, Y. Ishikawa, H. Itoh, G. E. W. Bauer, and L. W. Molenkamp, Phys. Rev. Lett. **97**, 046604 (2006).
[62] S. Onoda, N. Sugimoto, and N. Nagaosa, Phys. Rev. Lett. **97**, 126602 (2006).
[63] N. A. Sinitsyn, A. H. MacDonald, T. Jungwirth, V. K. Dugaev, and J. Sinova, Phys. Rev. B **75**, 045315 (2007).
[64] S. Y. Liu, Norman J. M. Horing, and X. L. Lei, Appl. Phys. Lett. **91**, 122508 (2007).
[65] C. P. Moca and D. C. Marinescu, New J. Phys. **9**, 343 (2007).
[66] M. F. Borunda, T. S. Nunner, T. Luck, N. A. Sinitsyn, C. Timm, J. Wunderlich, T. Jungwirth, A. H. MacDonald, and J. Sinova, Phys. Rev. Lett. **99**, 066604 (2007).
[67] T. Kato, Y. Ishikawa, H. Itoh, and J. Inoue, New J. Phys. **9**, 350 (2007).
[68] T. S. Nunner, N. A. Sinitsyn, M. F. Borunda, V. K. Dugaev, A. A. Kovalev, Ar. Abanov, C. Timm, T. Jungwirth, J. I. Inoue, A. H. MacDonald, and J. Sinova, Phys. Rev. B **76**, 235312 (2007).
[69] N. A. Sinitsyn, J. Phys. Condens. Matter **20**, 023201 (2008).
[70] S. Onoda, N. Sugimoto, and N. Nagaosa, Phys. Rev. B **77**, 165103 (2008).
[71] A. A. Kovalev, K. Vyborny, and J. Sinova, Phys. Rev. B **78**, 041305 (2008).
[72] L. Ren, J. Phys. Condens. Matter **20**, 075216 (2008).
[73] J. Inoue, T. Kato, G. E. W. Bauer, and L. W. Molenkamp, Semicond. Sci. Technol. **24**, 064003 (2009).
[74] A. A. Kovalev, Y. Tserkovnyak, K. Vyborny, and J. Sinova, Phys. Rev. B **79**, 195129 (2009).
[75] M. S. Garelli and J. Schliemann, Phys. Rev. B **80**, 155321 (2009).
[76] N. Nagaosa, J. Sinova, S. Onoda, A. H. MacDonald, and N. P. Ong, Rev. Mod. Phys. **82**, 1539 (2010).
[77] S. A. Yang, H. Pan, Y. Yao, and Q. Niu, Phys. Rev. B **83**, 125122 (2011).
[78] H. Y. Liu, Z. F. Hou, C. H. Hu, Y. Yang, and Z. Z. Zhu, J. Phys. Chem. C **116**, 18193 (2012).
[79] A. Sensharma and S. S. Mandal, Phys. Rev. B **86**, 165305 (2012).
[80] H. Z. Lu and S. Q. Shen, Phys. Rev. B **88**, 081304 (2013).
[81] I. A. Ado, I. A. Dmitriev, P. M. Ostrovsky, and M. Titov, Europhys. Lett. **111**, 37004 (2015).
[82] I. A. Ado, I. A. Dmitriev, P. M. Ostrovsky, and M. Titov, arXiv:1511.07413.
[83] R. Kubo, J. Phys. Soc. Jpn. **12**, 570 (1957).
[84] H. Fukuyama, H. Ebisawa, and Y. Wada, Prog. Theor. Phys. **42**, 494 (1969).
[85] H. Fukuyama, Prog. Theor. Phys. **42**, 1284 (1969).
[86] T. Ando, J. Phys. Soc. Jpn. **80**, 014707 (2011).
[87] T. Ando, J. Phys.: Conf. Ser. **302**, 012015 (2011).
[88] K. Ishikawa, Phys. Rev. Lett. **53**, 1615 (1984).
[89] E. Fradkin, E. Dagotto, and D. Boyanovsky, Phys. Rev. Lett. **57**, 2967 (1986).
[90] F. D. M. Haldane, Phys. Rev. Lett. **61**, 2015 (1988).
[91] D. Xiao, W. Yao, and Q. Niu, Phys. Rev. Lett. **99**, 236809 (2007).
[92] O. Narikiyo and K. Kuboki, J. Phys. Soc. Jpn. **62**, 1812 (1993).
[93] S.-D. Xiao, J.-H. Chen, S. Adam, E. D. Williams, and M. S. Fuhrer, Phys. Rev. B **82**, 041406 (2010).
[94] R. V. Gorbachev, J. C. W. Song, G. L. Yu, A. V. Kretinin, F. Withers, Y. Cao, A. Mishchenko, I. V. Grigorieva, K. S. Novoselov, L. S. Levitov, and A. K. Geim, Science **346**, 448 (2014).
[95] M.-Q. Sui, G.-R. Chen, L.-G. Ma, W.-Y. Shan, D. Tian, K. Watanabe, T. Taniguchi, X.-F. Jin, W. Yao, D. Xiao, and Y.-B. Zhang, Nat. Phys. **11**, 1027 (2015).
[96] Y. Shimazaki, M. Yamamoto, I. V. Borzenets, K. Watanabe, T. Taniguchi, and S. Tarucha, Nat. Phys. **11**, 1032 (2015).
[97] N. A. Sinitsyn, J. E. Hill, H. Min, J. Sinova, and A. H. MacDonald, Phys. Rev. Lett. **97**, 106804 (2006).
[98] E. O. Kane, J. Phys. Chem. Solids **1**, 249 (1957).
[99] L. M. Roth, B. Lax, and S. Zwerdling, Phys. Rev. **114**, 90 (1959).
[100] T. Ando, A. B. Fowler, and F. Stern, Rev. Mod. Phys. **54**, 437 (1982) and references cited therein.
[101] M. Cardona, J. Phys. Chem. Solids **24**, 1543 (1963).
[102] C. Hermann and C. Weisbuch, Phys. Rev. B **15**, 823 (1977).
[103] M. H. Weiler, *Semiconductors and Semimetals*, edited by R. K. Willardson and A. C. Beer (Academic Press, New York, 1981), Vol. 16, Chap. 3, p. 119.
[104] M. Cardona, N. E. Christensen, and G. Fasol, Phys. Rev. B **38**, 1806 (1988).
[105] P. Pfeffer and W. Zawadzki, Phys. Rev. B **41**, 1561 (1990).